OXFORD

PCARE requires coiled coil, RP62 kinase-binding and EVH1 domain-binding motifs for ciliary expansion

Tess A.V. Afanasyeva[1,2], Yan-Ting Schnellbach[1], Toby J. Gibson[3], Ronald Roepman [1,4] and Rob W.J. Collin [1,2,*]

[1]Department of Human Genetics, Radboud University Medical Center, Nijmegen, GA6525, The Netherlands
[2]Donders Institute for Brain, Cognition and Behaviour, Radboud University Medical Center, Nijmegen, GA6525, The Netherlands
[3]Structural and Computational Biology Unit, European Molecular Biology Laboratory, Heidelberg 69117, Germany
[4]Radboud Institute for Molecular Life Sciences, Radboud University Medical Center, Nijmegen, GA 6525, The Netherlands
*To whom correspondence should be addressed at: Donders Institute for Brain, Cognition and Behaviour, Radboud university medical center, Geert Grooteplein 10, 6525 GA Nijmegen, The Netherlands. Tel: +31 243613750; Fax: +31 243668752; Email: rob.collin@radboudumc.nl

Abstract

Retinitis pigmentosa (RP) is a genetically heterogeneous form of inherited retinal disease that leads to progressive visual impairment. One genetic subtype of RP, RP54, has been linked to mutations in *PCARE* (photoreceptor cilium actin regulator). We have recently shown that PCARE recruits WASF3 to the tip of a primary cilium, and thereby activates an Arp2/3 complex which results in the remodeling of actin filaments that drives the expansion of the ciliary tip membrane. On the basis of these findings, and the lack of proper photoreceptor development in mice lacking Pcare, we postulated that PCARE plays an important role in photoreceptor outer segment disk formation. In this study, we aimed to decipher the relationship between predicted structural and function amino acid motifs within PCARE and its function. Our results show that PCARE contains a predicted helical coiled coil domain together with evolutionary conserved binding sites for photoreceptor kinase MAK (type RP62), as well as EVH1 domain-binding linear motifs. Upon deletion of the helical domain, PCARE failed to localize to the cilia. Furthermore, upon deletion of the EVH1 domain-binding motifs separately or together, co-expression of mutant protein with WASF3 resulted in smaller ciliary tip membrane expansions. Finally, inactivation of the lipid modification on the cysteine residue at amino acid position 3 also caused a moderate decrease in the sizes of ciliary tip expansions. Taken together, our data illustrate the importance of amino acid motifs and domains within PCARE in fulfilling its physiological function.

Introduction

The vertebrate retina captures, amplifies and propagates light signals using intricately connected layers of photoreceptors, retinal neurons and optic nerve cells. This mechanism relies on the ability of photoreceptors to capture light photons and convert them into electrochemical signals via the action of opsin proteins that populate the stacked, disk-shaped membranes of photoreceptor outer segments (OSs). Photoreception and transduction place these OS under high oxidative stress, and therefore damaged components of the membrane disks require constitutive renewal of the OS. This is achieved by shedding of the OS tips at the rate of ∼10% per day, which is matched by OS biogenesis at the base (1). To support the highly metabolically active OS, a photoreceptor contains a biosynthetic inner segment that is connected to the OS by a microtubule-based bridge called the connecting cilium that is largely homologous to the transition zone of a primary non-motile cilium (2,3). The connecting cilium enters the OS in the region that cradles new opsin-loaded disks, which are formed by evagination and expansion of the ciliary plasma membrane (4,5). A branched F-actin

network localizes at the site of evagination; however, an exact mechanism of its involvement in disk morphogenesis remains elusive (6). Mutations in *PCARE* (photoreceptor cilium actin regulator) (*C2orf71*) have been linked to autosomal recessive retinitis pigmentosa type 54 (RP54) (7,8). PCARE has been found to localize to the evagination sites of photoreceptors where it interacts with WASF3 (WAVE3, SCAR3) protein (9). WASF3 is an actin modifier that is able to activate the Arp2/3 complex and facilitate assembly of a branched F-actin network (10,11). PCARE expression is specific to the retina; however, when PCARE is recombinantly expressed in cultured ciliated cells, it also localizes specifically to the cilium. Moreover, upon co-expression of WASF3, ciliary tip expansions appear that harbour both PCARE and WASF3 proteins. The formation of ciliary tip expansions is inhibited by F-actin poisons and siRNA-mediated downregulation of Arp2 expression (9).

This study aims to further investigate the role of PCARE in the actin dynamics of the ciliary tip by scrutinizing the structure of this novel protein. PCARE is an intrinsically disordered protein, which limits attempts to determine

its molecular structure using crystallographic methods (12). However, advances in the *in silico* predictions of protein structures allow us a glimpse into its structural and functional motifs. Previously, we described a tentative actin-binding WH2 short linear motif (SLiM) between amino acids 597 and 615 (9). WH2 is one of several SLiMs found in proteins that are involved in the regulation of actin filament assembly (13). However, when co-transfected with WASF3 in hTERT RPE-1 and IMCD-3 cell lines, PCARE lacking this WH2 motif retained the ability to form ciliary tip expansions (data not shown). This finding, together with an absence of robust motif representation in the eukaryotic linear motif (ELM) database (13) and low conservation score, prompted us to further study the structure–function relationship within the PCARE protein. We designed a bioinformatic study to predict evolutionary conserved amino acid motifs of PCARE. Subsequently, we revealed important functional amino acid motifs by expressing the PCARE mutant constructs lacking the motifs in hTERT RPE-1 and IMCD-3 cell lines and assessing their ability to localize to the cilia and form ciliary tip expansions. This work thereby points to a potential mechanism of actin dynamics during photoreceptor disc formation in health and disease.

Results

Bioinformatics analysis of PCARE protein showed structural and amino acid motifs potentially involved in interaction with actin and proteins involved in actin remodelling

PCARE is a retina-specific protein consisting of 1289 amino acids with a predicted molecular weight of 140 kDa. On the basis of the prediction using the DISOPRED and AlphaFold servers, the PCARE protein is mostly intrinsically disordered with a likely structured region between amino acids 171 and 338 (14,15). This region corresponds to a helical domain framed with two long helices forming an antiparallel coiled coil predicted with both the PSIPRED workbench and AlphaFold (16). The amino acid residue analyses showed no other strongly predicted structural domains (Supplementary Material, Fig. S1). Bioinformatic analysis revealed that the glycine residue at amino acid position 2 (p.Gly2) and the cysteine residue at amino acid position 3 (p.Cys3) may undergo myristoylation and palmitoylation lipid modifications, respectively (7). In the middle part of the protein, two target sites for the MAK (RP62) kinase were predicted (amino acid positions 513–516 and 577–580) and, in a proline-rich region, three enabled/VASP homology 1 domain (EVH1)-binding motifs (amino acids positions 805–809, 830–834 and 1056–1060).

PCARE mutants show stable protein expression comparable with wild-type

We modified recombinant *PCARE* cDNA to express a series of HA-tagged PCARE protein variants containing disrupted amino acid motifs (Fig. 1). To prevent lipid modification on the second glycine and third cysteine residues, the cDNA sequence was changed to encode the catalytically inert amino acid residue alanine at these positions. All other predicted amino acid motifs were disrupted by deleting the entire motif. We observed that the mutant *PCARE* constructs were stably expressed when transfected into HEK293T cells and their levels of expression were comparable to that of the recombinant wild-type protein (Fig. 2).

Disturbance of predicted PCARE motifs differentially affects ciliary characteristics

When transfected into hTERT RPE-1 cells, wild-type PCARE has been shown to localize along the cilia (9). We repeated this experiment with wild-type and mutant PCARE isoforms and observed ciliary localization for each of them except for the mutant harbouring the helix domain deletion (PCAREΔhelix) where the protein localized into the cytosol only (Fig. 3).

When co-transfected with WASF3, PCARE induces the formation of ciliary tip expansions. We classified three ciliary phenotypes: type 1, where PCARE and WASF3 co-localize into the cilia and form expansions of the ciliary tip; type 2, where the proteins co-localize to the cilia but form no expansions and type 3, where cilia also appear normal but PCARE and WASF3 retain within the cytosol and/or nucleus (Fig. 4, Supplementary Material, Fig. S3). With wild-type PCARE, 50% of the colocalization events resulted in the formation of ciliary expansions of type 1 per total double-positive cilia ($n = 271$ number of double-positive cilia counted, SD = 7.8%). Mutant constructs formed less of type 1 expansions, for example, PCAREΔEVH1a, b and c formed 39%, 37% and 48% of type 1 expansions, respectively ($n = 71$, SD = 8.8%, $n = 70$, SD = 8.5% and $n = 62$, SD = 10.5%), whereas PCAREΔRP62a and PCAREΔRP62b ($n = 71$, SD = 10.0% and $n = 66$, SD = 9.6%) formed 48% and 42% of expansion, respectively (Fig. 4A–C). We observed the second most prominent decrease in type 1 expansions in PCAREΔEVH1a–c (14%, $n = 61$, SD = 5.2%). PCAREΔhelix ($n = 34$) failed to localize into the cilia and thus did not form expansions at all.

Furthermore, we quantified the size of the ciliary tip expansions formed upon co-transfection of PCARE mutant constructs with WASF3 in hTERT RPE-1 cells. We observed the mean expansion size of wild-type PCARE to correlate with previous observations (0.97 μm^2, $n = 117$, SD = 0.4 μm^2) (9). Our results showed that most mutated constructs formed smaller expansions than the wild-type. From those, the PCAREΔEVH1a and b constructs formed significantly smaller expansions with means at 0.82 μm^2 and 0.75 μm^2, respectively ($n = 73$, SD = 19 μm^2, $P = 0.001$ and $n = 37$, SD = 0.2 μm^2, $P < 0.0001$). The triple-deletion PCAREΔEVH1a–c showed the smallest mean expansion size of 0.71 μm^2 ($n = 10$, SD = 0.22 μm^2, $P = 0.006$). Also, a removal of lipid modification from p.Cys3 might result in a decreased expansion size (size = 0.84 μm^2, $n = 36$, SD = 0.28 μm^2, $P = 0.035$) (Fig. 4D).
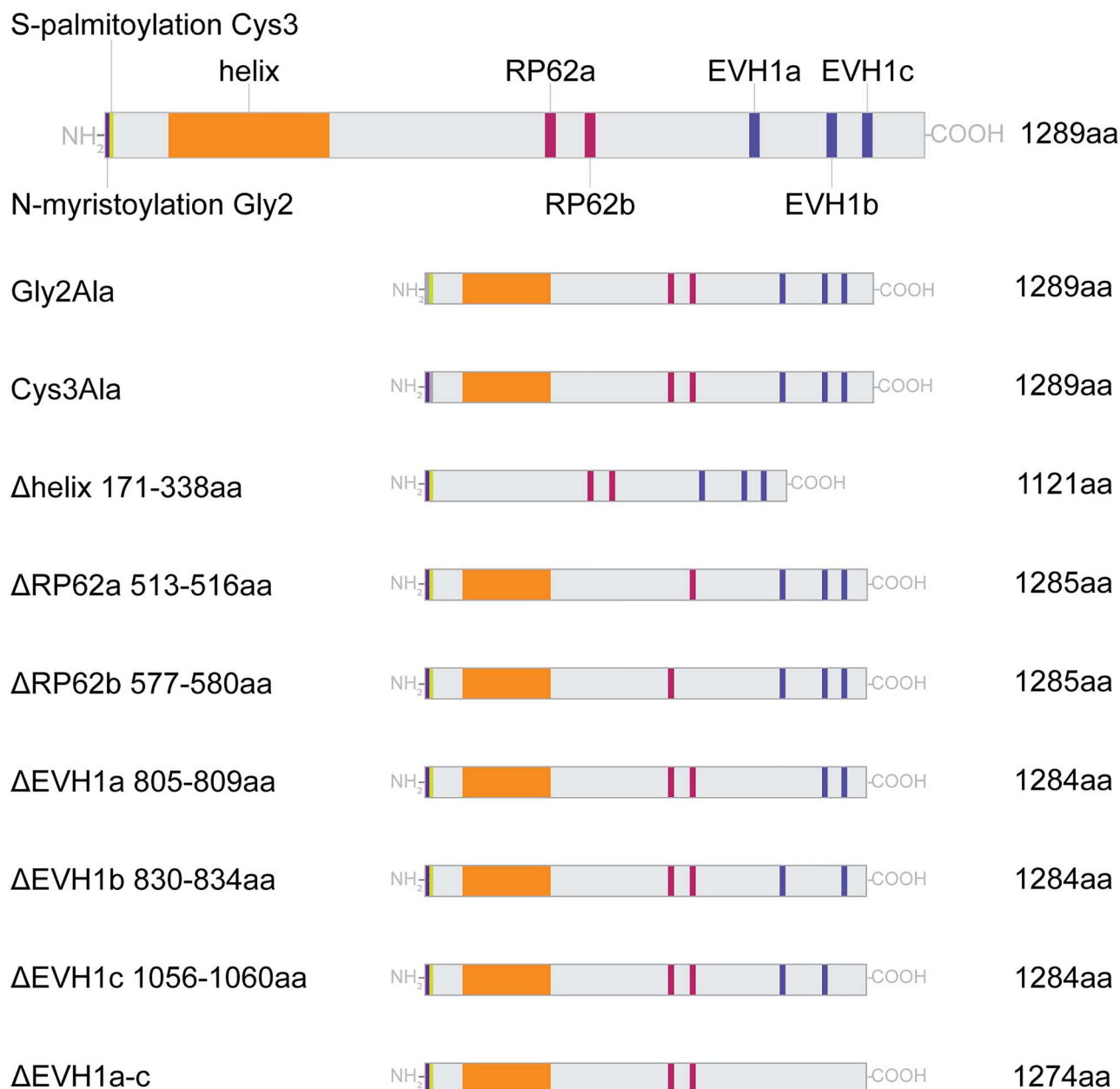
Figure 1. Bioinformatic analysis shows structural and functional amino acid motifs in PCARE protein. *PCARE* encodes a protein of 1289 amino acids. At the N-terminus of PCARE, the glycine residue at amino acid position 2 (p.Gly2), and the cysteine residue at amino acid position 3 (p.Cys3) exhibit tentative palmitoylation and myristoylation lipid modifications, respectively. As predicted with DISOPRED server, a helical structural domain is located between amino acids 171 and 338. Using Jalview, the following conserved SLiMs were predicted: two RP62 kinase-binding motifs, and three EVH1 domain-binding motifs. To generate PCARE mutant proteins, the p.Gly2 and p.Cys3 residues were substituted by the inactive amino acid alanine residue, whereas predicted protein domains that are annotated in this schematic were deleted via site-directed mutagenesis, including one mutant in which all three EVH1 domain-binding motifs were deleted.

The absence of lipid modification on p.Gly2 or deletions of RP62 candidate phosphomotifs did not exhibit a statistically significant difference in ciliary expansion size (Table 1).

Transfection of PCARE mutant constructs into stable IMCD-3 expressing WASF3 confirms decreased ability to form tip expansions

To minimize the variability of the double-transfection experimental design, we also generated IMCD-3 cell lines stably expressing WASF3 that allowed for a standardized level of WASF3 expression between samples (Supplementary Material, Fig. S2). In the IMCD-3 cells, the average percentage of cilia with type 1 phenotype increased by 12% while type 3 decreased by 9%, whereas the average SD of expansion sizes decreased by 16%. Most of the results observed in IMCD-3 cells stably expressing WASF3 followed the trends of hTERT RPE1 cell results (Fig. 5). For example, removal of lipid modification from the cysteine residue at amino acid position 3 also showed a decrease in the ciliary tip expansion sizes
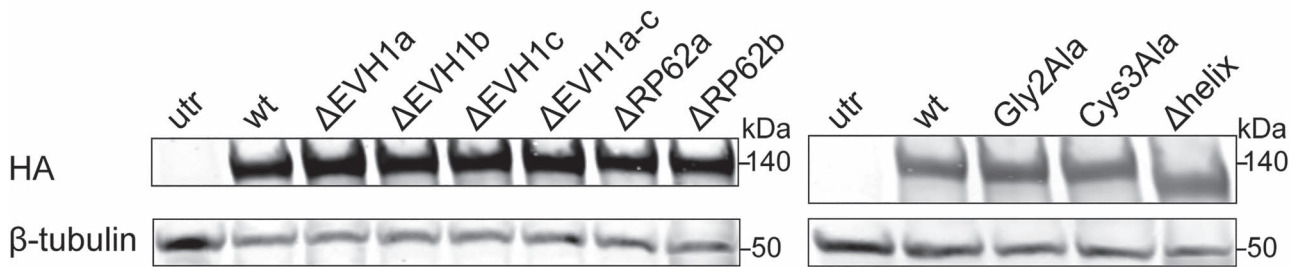
Figure 2. PCARE mutants are expressed and stable. Wild-type and mutant PCARE constructs were transfected in HEK293T cells. Western blot analysis revealed stable expression of all PCARE constructs. Wild-type PCARE protein has a molecular weight of 140 kDa, the molecular weight of mutant PCARE proteins is approximately the same, except for the mutant carrying the helix deletion which is smaller. Tubulin was loaded for control of the total amount of protein.
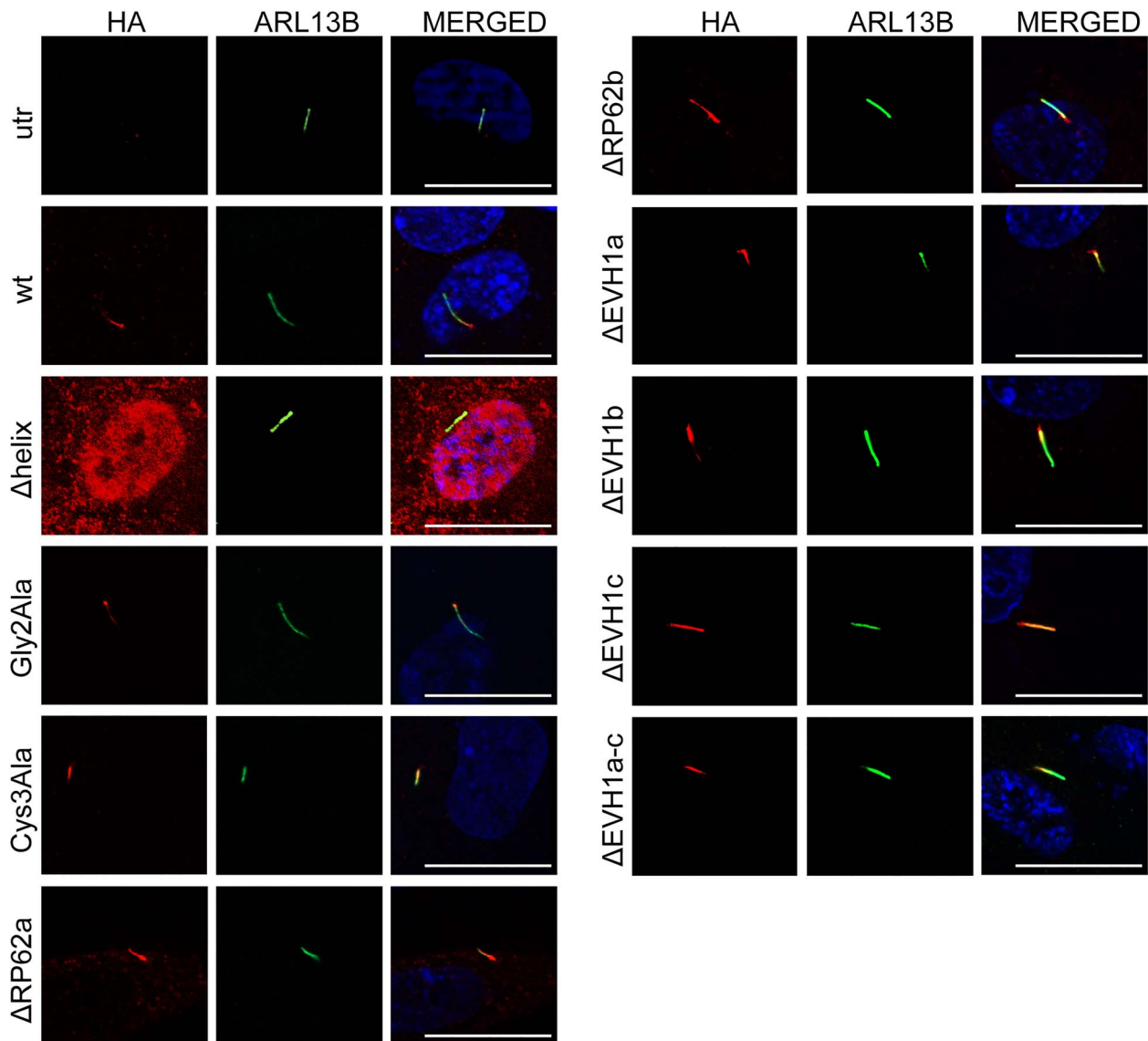

Figure 3. Mutant PCARE isoforms, except for PCAREΔhelix, localize to the cilia. Wild-type and mutant HA-tagged PCARE constructs were overexpressed in hTERT RPE-1 cells. Upon visualization with an anti-HA antibody, wild-type HA-tagged PCARE and PCARE mutant constructs except for PCAREΔhelix are co-localized with ciliary axoneme staining (anti-HA in red, ARL13B in green, DAPI in blue). All scale bars are 20 μm.

$(0.76 \ \mu\text{m}^2, n = 133, \text{SD} = 0.29, P = 0.024)$. As in the hTERT RPE-1 cells, PCAREΔEVH1a formed significantly smaller mean expansion size of 0.69 μm^2 ($n = 147$, SD = 0.22, $P < 0.0001$). Also, the observation was consistent for PCAREΔEVH1a–c ($0.72 \ \mu\text{m}^2, n = 43, \text{SD} = 0.18 \ \mu\text{m}^2, P = 0.006$). In contrast to hTERT-RPE1, no effect on mean expansion size was observed for PCAREΔEVH1b ($0.77 \ \mu\text{m}^2$, SD = 0.24 μm^2, $P = 0.052$), but deletion of each MAK/RP62
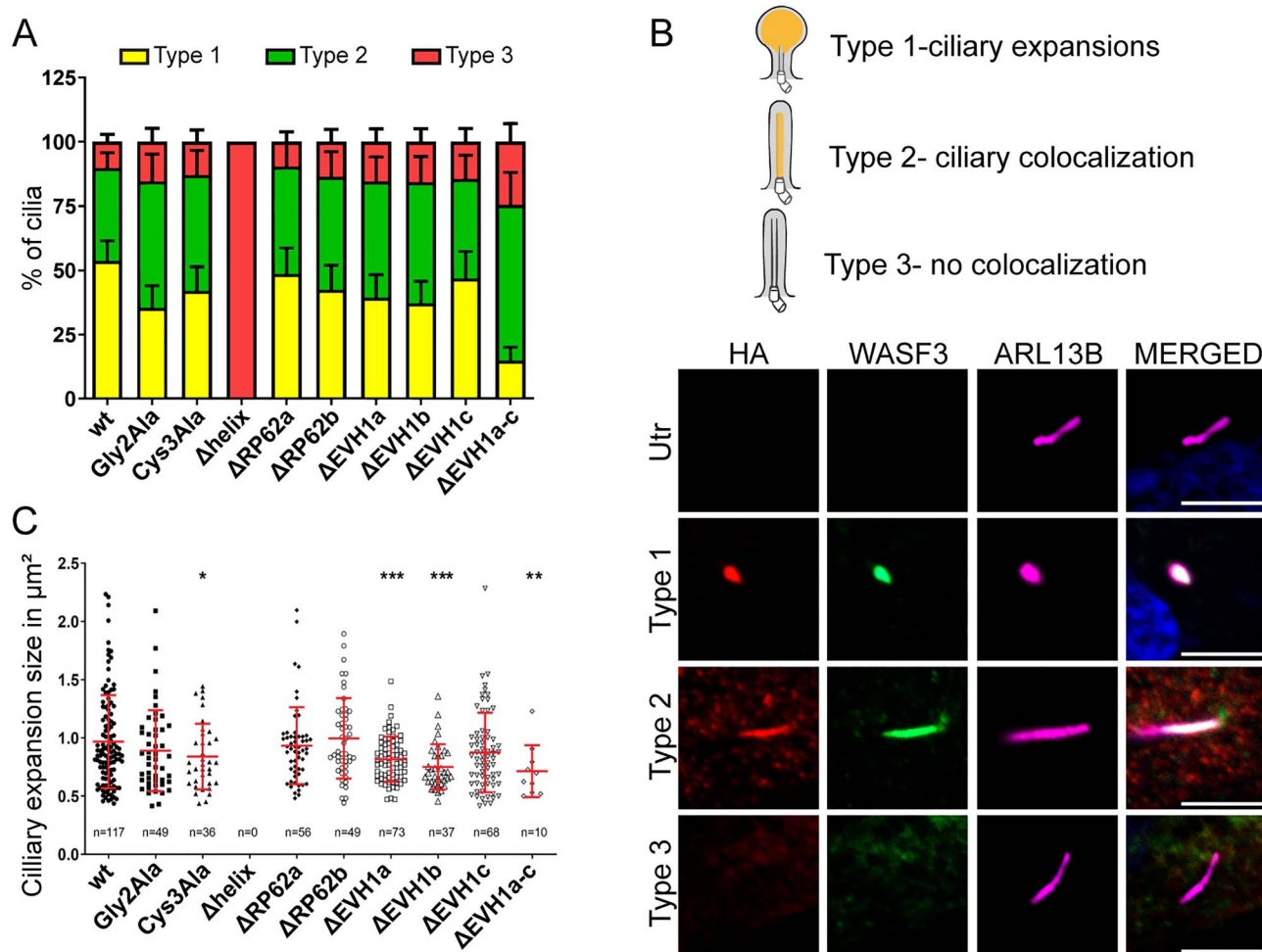
Figure 4. PCARE mutants differentially form ciliary expansions upon co-transfection with WASF3 in hTERT RPE-1. (**A**) When counted in the IHC slide and quantified, with wild-type PCARE normalized to hundred percent, all PCARE mutants generated less ciliary tip expansions than the wild-type (type 1 in yellow, type 2 in green, type 3 in red). (**B**) hTERT RPE-1 cells were transfected with 3×HA-PCARE (wild-type or mutant) and 3×FLAG-WASF3 constructs in equal amounts. Three distinct types of the ciliary tip expansions can be distinguished: type 1, where PCARE and WASF3 co-localize into the cilia and form expansions of the ciliary tip, type 2, where the proteins co-localize to the cilia but formed no expansions and, finally, type 3, where the proteins are retained in the cytosol (3×HA-PCARE in green, WASF3 in red, ARL13B in magenta, DAPI in blue). Untransfected cells (Utr) are shown as a negative control. Scale bars 5 μm. (**C**) The sizes of the ciliary tip expansions of type 1 were counted and quantified using an automated Fiji script. The triple-deletion PCAREΔEVH1a–c and single-deletions of PCAREΔEVH1a and PCAREΔEVH1b showed a significant decrease in the size of the expansion tip (***$P \leq 0.001$, **$P \leq 0.01$, *$P \leq 0.05$, red line shows mean and SD).

Table 1. Means, standard deviations, numbers and *P*-values of ciliary tip expansion sizes formed by PCARE constructs

PCARE construct	hTERT RPE-1				IMCD-3			
	Mean (μm^2)	SD (μm^2)	n	P-value	Mean (μm^2)	SD (μm^2)	n	P-value
Wild-type	0.97	0.40	117		0.83	0.28	151	
p.Gly2Ala	0.89	0.35	49	0.215	0.83	0.30	138	0.867
p.Cys3Ala	0.84	0.28	36	0.035	0.76	0.29	133	0.024
Δhelix	0.00	0.00	0	n/a	0.00	0.00	0	n/a
ΔRP62a	0.93	0.33	56	0.549	0.72	0.22	109	0.0005
ΔRP62b	1.00	0.35	49	0.646	0.72	0.25	245	<0.0001
ΔEVH1a	0.82	0.20	73	0.001	0.69	0.22	147	<0.0001
ΔEVH1b	0.75	0.20	37	<0.0001	0.77	0.24	144	0.052
ΔEVH1c	0.87	0.34	68	0.096	0.75	0.26	115	0.014
ΔEVH1a-c	0.71	0.22	10	0.006	0.72	0.18	44	0.002

candidate phosphomotif resulted in a statistically significant mean decrease (0.72 μm^2, $n = 109$, SD = 0.22, $P = 0.0005$ and 0.72 μm^2, $n = 245$, SD = 0.25, $P < 0.0001$).

Furthermore, for PCAREΔEVH1c, a decrease of expansion size was also observed (mean = 0.75 μm^2, $n = 115$, SD = 0.26, $P = 0.014$) (Table 1).
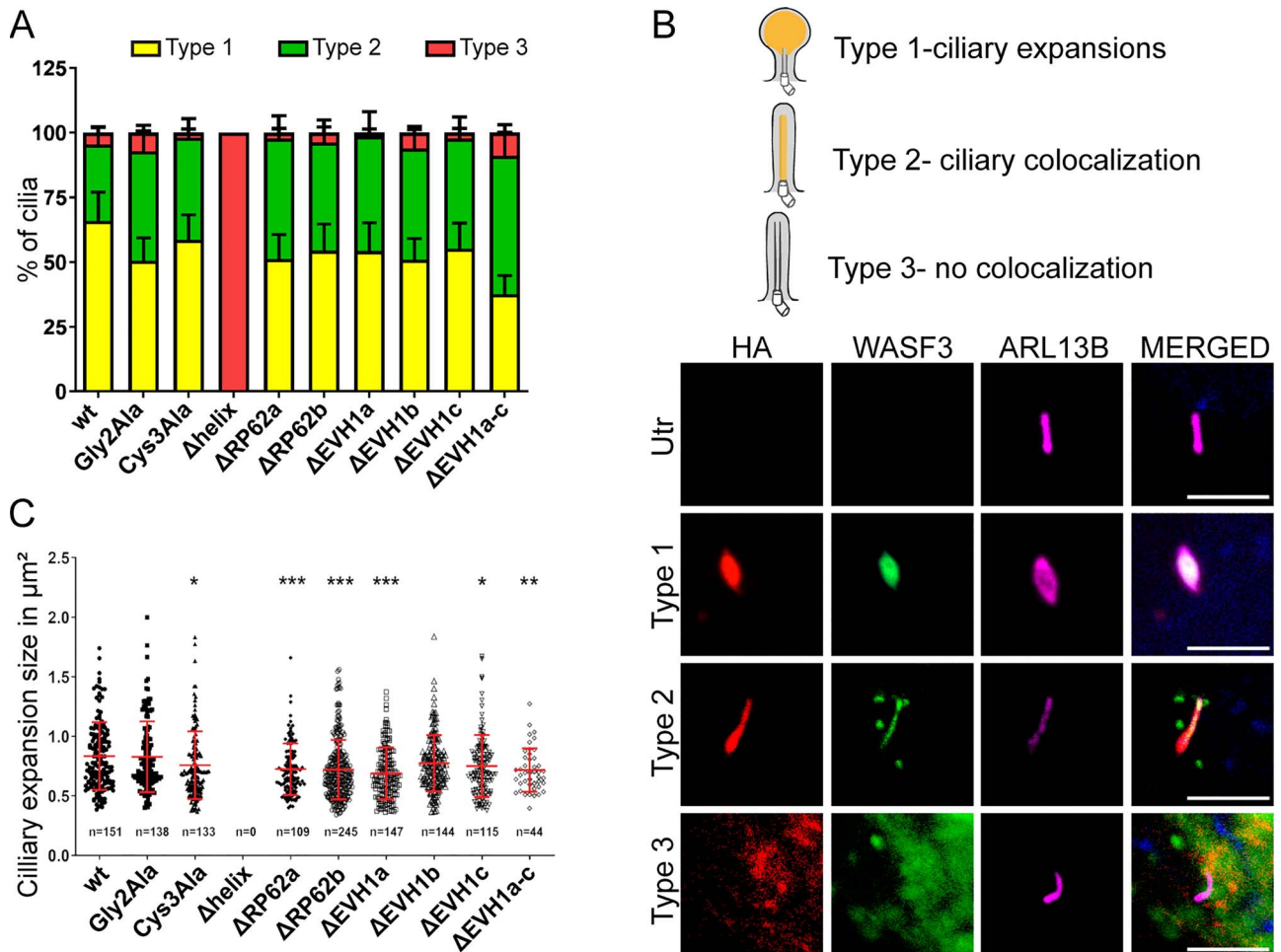
Figure 5. PCARE mutants form ciliary expansions when co-expressed with WASF3 in IMCD-3 stable cell line. (**A**) When counted in the IHC slide and quantified, with wild-type PCARE normalized to hundred percent, all PCARE mutants generated less ciliary tip expansions than the wild-type (type 1 in yellow, type 2 in green, type 3 in red). (**B**) IMCD-3 cells stably expressing FLAG-tagged WASF3 were transfected with 3×HA-PCARE (wild-type or mutant) constructs. Three distinct types of the ciliary tip expansions can be distinguished: type 1, where PCARE and WASF3 co-localize into the cilia and form expansions of the ciliary tip, type 2, where the proteins co-localize to the cilia but formed no expansions and, finally, type 3, where the proteins co-localize into the cytosol (3×HA-PCARE in green, WASF3 in red, ARL13B in magenta, DAPI in blue). Untransfected cells (Utr) are shown as a negative control. Scale bars 5 μm. (**C**) The sizes of the ciliary tip expansions of type 1 were counted and quantified using an automated Fiji script. The removal of lipid modification from the p.Cys3, PCAREΔEVH1a and PCAREΔEVH1a–c led to a significant decrease in the ciliary tip expansion sizes. (***$P \leq 0.001$, **$P \leq 0.01$, *$P \leq 0.05$, red line shows mean and SD).

Discussion

Mutations in PCARE are causative for retinal ciliopathy RP54 (7,8). Recently, we observed that PCARE localizes at the initiation site of new OS disks within photoreceptors and proposed its role in protein transport and actin remodelling that is required to form OS disks (9). We identified candidate SLiM motifs of PCARE that may be relevant for interactions with actin or actin modifiers and generated stable PCARE protein mutants with deletion or inactivation of these motifs. Our data strongly suggest the importance of the alpha-helix domain for PCARE ciliary trafficking and EVH1 domain-binding motifs and myristoylation on the third cysteine for modification of the actin filament network in the ciliary tip.

The aim of this study was to investigate the structure–function relationship within PCARE with regard to its ability to regulate actin dynamics. To address this, we performed a bioinformatics analysis of PCARE

protein structure to find evolutionary conserved structural and functional amino acid motifs. From the list of predicted SLiMs, we selected the motifs that are potentially involved in interaction with actin or with other proteins involved in actin remodelling. We identified two target sites for a photoreceptor cilium-associated MAK/RP62 that phosphorylates serine and threonine residues (17). Dysfunction of MAK kinase is linked to structural defects in photoreceptor cilia and recessive retinitis pigmentosa (18–20). MAK knockout mice retina shows elongated cilia, rhodopsin accumulation and photoreceptor degeneration (21). Furthermore, we identified three EVH1 domain-binding SLiMs that are specific to proteins that are involved in actin-based cytoskeleton reorganization, actin dynamics modulation and actin motility (22–24). We also modified amino acids (p.Gly2 and p.Cys3) at the N-terminus of PCARE, because of their known role as a lipid modification

sites in transport and membrane localization of proteins (17). Finally, PCARE contains one predicted alpha-helical domain, one of the most common secondary structure motifs found within proteins (18). To access the function of each of these motifs, we generated PCARE mutant constructs with deletion or inactivation of the motifs of interest on the basis of wild-type PCARE cDNA.

To determine the influence of the predicted amino acid motifs on the PCARE stability, we expressed the PCARE mutant constructs in HEK293T cells and assessed PCARE expression levels. All mutant proteins were expressed at levels comparable to wild-type PCARE. Furthermore, to elucidate the function of the selected motifs in PCARE ciliary trafficking, we investigated the localization pattern of PCARE mutants in ciliated hTERT RPE-1 and IMCD-3 cells. Previously, we showed that, when separated into arbitrarily chosen fragments, the most N-terminal fragment of PCARE, which harbours the alpha-helical coiled coil domain, localizes to the basal body and axoneme of the cilia and is sufficient to transport WASF3 into the cilia to form ciliary tip expansions (9). Interestingly, the most C-terminal fragment of PCARE alone was also capable of localization into the ciliary axoneme. Here, we showed that full-size PCARE lacking the helix domain failed to localize to the cilia. This finding hints towards a crucial role that the minimal structural organization of PCARE has in its ciliary localization and further work is required to establish the exact role of the coiled coil domain in PCARE trafficking. Moreover, myristoylation and palmitoylation were predicted at the N-terminus of PCARE, modifications that are known to play a role in ciliary trafficking in *Trypanosoma brucei* and in eukaryotic cells (19,20). N-myristoylation on p.Gly2 is a protein modification where 14-carbon saturated fatty acid myristate is covalently attached to the N-terminal Gly (exposed after removal of p.Met1) of the target protein catalyzed by N-terminal myristoyltransferases. On p.Cys3, palmitoylation where 16-carbon fatty acid palmitate is covalently attached to a cysteine residue is predicted, a process that is catalyzed by the N-terminal palmitoyl acyltransferases. Myristoylation at the N-terminus also facilitates palmitoylation (25,26). The lipid-modified protein is directed to a membrane by the action of N-myristoylation, but palmitoylation is required for stable anchoring to the phospholipid bilayer (27). In X-linked retinitis pigmentosa protein 2 (RP2), myristoylation alone was not sufficient to traffic amino acid residues 1 to 16 RP2 to the cilia (20). We deactivated palmitoylation on Gly2 or myristoylation on Cys3 by Gly-to-Ala or Cys-to-Ala substitutions, but observed no effect on the ciliary trafficking. Further analysis of human retinal-organoid derived, or murine purified PCARE protein, for example by mass spectrometry, would be required to determine if p.Gly2 or p.Cys3 is respectively myristoylated or palmitoylated *in vivo*. Taken together, our data show that all PCARE mutants except for PCAREΔhelix localized to the cilia, suggesting redundancy or potentially undiscovered amino acid motifs to play a role in ciliary trafficking of PCARE.

Next, we accessed the frequency and size of ciliary tip expansions generated by PCARE mutant proteins when co-expressed with WASF3, either via double transfection of both proteins in hTERT RPE-1 cells, or by a single transfection of PCARE in IMCD-3 cells stably expressing WASF3. All mutants showed a decreased frequency of ciliary tip expansions compared with the wild-type PCARE. In IMCD-3 cells stably expressing WASF3, there is a general increase in the ability to form ciliary tip expansions for all protein variants compared with double-transfected hTERT RPE-1. Compared with the wild-type, both PCARE (p.Gly2Ala), where the myristoylation was inactivated and PCARE (p.Cys3Ala), where the palmitoylation was inactivated, showed a lower number of ciliary tip expansions of type 1. When quantifying the sizes of the ciliary tip expansions, the deactivation of myristoylation had no statistically significant effect but the deactivation of palmitoylation seemed to have negatively affected the ability of PCARE to form ciliary tip expansions. Potentially, the palmitoylation-affected mutant impaired membrane anchoring and, thus, fewer units of the protein complex may reach the ciliary tip leading to fewer and smaller bulges.

Deletion of the EVH1 domain-binding motifs, both sequentially and concurrently, also resulted in fewer and smaller ciliary tip expansions in both hTERT RPE-1 and IMCD-3 cell lines. Analysis of the sequential deletions showed that the deletion of the most evolutionary conserved EVH1b motif affects the tip expansions most strongly in both cell lines. Analysis of concurrent EVH1 domain-binding SLiM deletions showed the strongest effect when all three EVH1 domain-binding motifs were deleted simultaneously. Although this effect is stronger than that of the individual deletions, more research should be done to explore a potential synergistic effect of the EVH1 deletions. Putative EVH1 domain-binding motifs would allow PCARE to interact with proteins that have the EVH1 (WH1, RanBP1-WASP; Pfam:PF00568) domain that is present in species ranging from yeast to mammals. Such proteins are involved in a wide range of signalling, nuclear transport and cytoskeletal events. Many EVH1-containing proteins are actin interactors and participate in actin cytoskeleton organization. The EVH1 domain-binding motifs of PCARE consist of five amino acid stretches containing three or more proline residues and resemble the EVH1 domain-binding motifs in other proteins such as the Ena/VASP family proteins, which are thought to assist in actin filament formation by profilin-actin complexes to their proline-rich binding partners (28). For example, EVH1-binding motifs might facilitate interaction with Protein-enabled homolog (ENAH) and Vasodilator stimulated phosphoprotein (VASP) PCARE interactor proteins that we have identified in yeast two-hybrid screening and tandem affinity purification studies (9). A very recent structural study has shown that PCARE binds with a high affinity to the EVH1 domain of

the protein ENAH, which as noted we had previously identified as a PCARE interactor, that plays a role in actin polymerization and cytoskeletal remodelling (29). Taken together, these studies establish that PCARE acts through ENAH to regulate actin filament assembly in the eye photoreceptor cilium.

MAK/RP62 kinase candidate phosphorylation site mutants PCAREΔRP62a and PCAREΔRP62b showed a similar frequency of expansion formation to the wild-type. Possibly, that although MAK/RP62 kinase is crucial for ciliary length and retinal health, it does not directly affect actin network polymerization via PCARE. However, for PCAREΔRP62a and PCAREΔRP62b, we observed a subtle but significant difference between hTERT RPE-1 and IMCD-3 cell lines in the ciliary tip expansion size.

When comparing the results obtained in IMCD-3 and hTERT RPE-1 cells, it is clear that although most of the findings were evident in both cell lines, the immortalized cell line models might provide contradictive readouts. Being derived from mouse kidney or human retinal epithelial cells, these models cannot fully represent the function of photoreceptor cells. Therefore, further confirmation of PCARE protein's functions is required with model systems that more faithfully represent the human retina, for example in human iPSC-derived retinal organoids (30). The recent advances in these techniques allow for precise editing of the gene of interest to induce mutations via the CRISPR-Cas9 editing machinery, which can be further studied at a different level of complexity such as protein expression, morphology or even function (20).

To conclude, all PCARE mutants that localized into the cilia formed ciliary tip expansions, suggesting that PCARE contains a redundancy of amino acid motifs via which it can interact with actin modulators and that it may interact with multiple actin-modulators. Our data also pinpoint the prominent role of proteins with EVH1 domains and hint towards the importance of palmitoylation lipid modification in the PCARE–actin interactions. This work presents a first glance at the importance of amino acid modules in PCARE and expands upon their structure and function in relationship to actin network modification, paving the way for improved understanding of mechanisms that underlie PCARE-associated retinal disease, as well as the formation of the OS disks of photoreceptors.

Materials And Methods
Bioinformatic prediction of structural and functional amino acid motifs within PCARE protein

The human PCARE SEQUENCE (UniProt:A6NGG8) was submitted to the Eukaryotic Linear Motif resource (http://elm.eu.org) server (13). Among the candidate matches were three proline-rich EVH1-binding SLiMs (805–809, 830–834, 1056–1060: http://elm.eu.org/elms/LIG_EVH1_1.html). A multiple sequence alignment of vertebrate PCARE sequences was prepared and visualized with Jalview (31). All vertebrate PCARE sequences had multiple EVH1 motifs, with some variation in number and positioning, as often occurs with SLiMs. Since these candidates are in regions of predicted native disorder, amino acid conservation is driven by functional, not structural selection: Thus, these motifs are strong candidates for actin-regulatory function via EVH1 domain binding (32). By visual inspection, we also noted two conserved RPx[ST] motifs (513–516, 577–580) that are candidate phosphorylation sites (33) for the MAK (RP62) ciliary protein kinase (UniProt:P20794) required for long-term photoreceptor survival (33). All vertebrate PCARE sequences begin with the residues MetGlyCys indicative of N-terminal myristoylation and prenylation. Structural context was provided by native disorder predictors IUPRED (34) and DISOPRED (14) and the PSIPRED 4.0 (http://bioinf.cs.ucl.ac.uk/psipred/) workbench (16). More recently, the structural context was re-evaluated with AlphaFold (35), supporting the disorder predictions and providing high confidence assignment for the long helices (171 and 338) as an anti-parallel coiled coil pair (see Supplementary Material, Fig. S1).

Generation of mutant *PCARE* constructs

Human *C2orf71/PCARE* [NCBI GeneID:388939] full-length cDNA was obtained by PCR using Human Retina Marathon®-Ready cDNA (Clontech) and cloned into Gateway™ pDONR201 vector (Thermo Fisher) as previously described (9). PCARE mutant constructs lacking functional and structural motifs were constructed by performing site-directed mutagenesis on pDONR with cloned *PCARE* cDNA construct with primer pairs that introduced deletions of nucleotide coding for the amino acid motifs via PCR amplification with Q5 High-fidelity DNA polymerase (New England Biolabs, M0491L). PCR reactions were performed using 0.2 ml PCR tubes in a final volume of 50 μl including the following components: 50 ng of template DNA, 0.5 μM of each primer (forward and reverse), 200 μM of each dNTPs, 1× Q5 Buffer and 1.6 U of Q5 High-fidelity DNA polymerase. 30 cycles of amplification were carried out under the following conditions: initial denaturation at 98°C for 4 min, denaturation at 98°C for 30 s, annealing at 50°C for 30 s and extension at 72°C for 3 min, following by final extension at 72°C for 7 min. Primer sequences are listed in Supplementary Material, Table S1. Parental plasmid DNA was eliminated by DpnI treatment (1 μl of 20 U/μl) (New England Biolabs, R0176S) of a 10-μl aliquot of the linear amplification reaction for 1 at 37°C. DNA was then directly transformed to competent *Escherichia coli* DH5α cells and purified with NucleoSpin Plasmid EasyPure (BIOKÉ, MN740727). Constructs were checked for deletions by amplification of the 200 nucleotide target region around the deletion with forward and reverse primers with *Taq* polymerase (Roche, 11 647 687 001). Thirty-five cycles of amplification were carried out under the following conditions: initial denaturation at 94°C

for 5 min, denaturation at 94°C for 30 s, annealing at 58°C for 30 s and extension at 72°C for 20 s, following by final extension at 72°C for 5 min. At the completion of the PCR, fragments were separated on 2.5% agarose gels containing 0.5 μg/ml ethidium bromide and further verified by Sanger sequencing. The entire coding region of constructs containing the modification of interest was verified by Sanger sequencing. The obtained entry clones were used to generate expression clones containing 3×HA tag using Gateway Technology (Life Technologies) and according to the manufacturer's instructions.

Generation of a stable IMCD-3 cell line expressing WASF3

To generate a stable cell line expressing FLAG-tagged WASF3, IMCD-3 FlpIn cells (a kind gift from Dr M.V. Nachury) that contain a stably integrated FRT cassette were used as parental line and cultured as wild-type IMCD-3 cells as aforementioned. Stable cell lines were generated as previously described (36). In short, the parental line was co-transfected with pOG44 construct (Addgene) coding an FLP recombinase together with the construct of WASF3 [generated by replacing the GFP for the N-terminal Strep-FLAG epitope of the pgLAP1 vector (Addgene)] using Lipofectamine 2000 (Thermo Fisher, 11 668 019) according to the manufacturer's instructions. pENTRWASF3 [NP_001278894.1] was a generous gift from Prof. N. Katsanis (Duke University School of Medicine, Durham, US). Successful stable genomic integration after selection with media supplemented with 400 μg/ml hygromycin (Sigma-Aldrich, H0654) was confirmed by analysis of the expression of FLAG-WASF3 by western blot analysis with primary antibodies: rabbit anti-flag (clone 11, Sigma-Aldrich, 1:400, F7425-.2MG) and mouse anti-alpha-tubulin (Abcam, 1:1000, AB15568) and by immunofluorescence with primary antibodies: goat anti-WASF3 (R&D systems, 1:300, AF5515) and mouse anti-ARL13 B (NeuroMab, 1:250, 73–287). Primary antibodies were visualized using the following secondary antibodies in western blot: goat anti-mouse, IRDye 680 (Molecular Probes, 1:10 000, A21057) and goat anti-rabbit, IRDye 800 (LI-COR, 1:10 000, 926–3221). Primary antibodies were visualized using the following secondary antibodies in immunofluorescence: donkey anti-goat, Alexa Fluor 568 (Molecular Probes, 1:500, A11057), and donkey anti-mouse, Alexa Fluor 488 (Life Technologies, 1:500, A21202).

Cell culture

For western blotting, HEK293T cells were grown in DMEM medium (Sigma-Aldrich, D0819) supplemented with 10% FCS (Sigma-Aldrich, F0392), 1% sodium pyruvate (Sigma-Aldrich, S8636) and 1% penicillin/streptavidin (Sigma-Aldrich, P4333). For immunofluorescence analysis, hTERT RPE-1 and IMCD-3 cells were grown in DMEM/F12, supplemented with 10% FCS (Sigma-Aldrich, F0392), 1% sodium pyruvate (Sigma-Aldrich, S8636) and 1% penicillin/streptavidin (Sigma Aldrich, P4333). IMCD-3 cells stably expressing WASF3 were further

supplemented with 400 g/μl hygromycin (Sigma-Aldrich, H0654). All cells were cultured at 37°C and under 5% CO2.

Western blot analysis

HEK293T cells were seeded and expanded for 5 h, then transfected with the appropriate construct using FuGENE HD Transfection Reagent (Promega, E2311) according to the manufacturer's instructions. 96 h later, cells were detached with trypsin and centrifuged at 10 000 g for 10 min. Cellular pellets were resuspended in 150 μl RIPA buffer (50 mM Tris pH 7.5, 1 mM EDTA, 150 mM NaCl, 0.5% Na-Deoxycholate, 1% NP-40 plus protease inhibitors) rotating for 20 min at 4°C. Cells were sonicated for 15 s and centrifuged for 5 min at 12 000 g, 4°C to remove cell debris and nuclei. The supernatant was mixed with Laemmli sample buffer (Bio-Rad, 1 610 737) supplemented with 0.1 M DTT (Sigma-Aldrich, 43 816) and heated at 70°C for 10 min. To standardize the amount of protein per sample, BCA assay was performed using the PierceTM BCA Protein Assay kit (Thermo Fisher, 23 225) according to the manufacturer's instructions. Cellular proteins were separated by SDS-PAGE with a 3–8% Tris-Acetate Gel (Invitrogen, EA0375BOX) and transferred to a nitrocellulose membrane (GE healthcare, 10 600 007) using standard protocols. The following primary antibodies were used: mouse anti-HA (Sigma-Aldrich, 1:1000, H9658) and rabbit anti-beta-tubulin (Abcam, 1:1000, AB15568). Primary antibodies were visualized using the following secondary antibodies: goat anti-mouse, IRDye 680 (Molecular Probes, 1:10 000, A21057) and goat anti-rabbit, IRDye 800 (LI-COR, 1:10 000, 926–3221). Images of the western blot were acquired using the Odyssey machine (Li-cor Biosciences, Bad Homburg, Germany) and quantified using software Fiji version 1.53c (37). The PCARE protein signal was normalized to beta-tubulin.

Immunocytochemistry

For immunofluorescence imaging, hTERT RPE-1 and IMCD-3 cells were plated on glass coverslips and, 24 h later, were starved to induce cilia formation by feeding with DMEM medium (Sigma-Aldrich, D0819) supplemented with 1% sodium pyruvate (Sigma-Aldrich, S8636), 1% penicillin/streptavidin (Sigma-Aldrich, P4333) and 0.2% FCS (Sigma-Aldrich, F0392). hTERT RPE-1 cells were transfected with 450 ng each of 3×HA-PCARE and 3×FLAG-WASF3 construct or with 650 ng of 3×HA-PCARE, whereas IMCD-3 cells stably expressing WASF3 were transfected with 650 ng DNA of 3×HA-PCARE construct using Lipofectamine 2000 (Thermo Fisher, 11 668 019), according to the manufacturer's instructions. Twenty-four hours post-transfection cells were fixed for 20 min at room temperature, followed by 1% Triton-X-100 treatment for 3 min and blocking in 2% BSA for 20 min. Subsequently, cells were incubated with primary antibodies diluted in blocking solution for 1 h. Following primary antibodies were used for staining single transfected cells: mouse anti-HA (Sigma-Aldrich,

1:500, H9658) and rabbit anti-ARL13 B (Sanbio, 1:500, 17 711–1-AP). Following primary antibodies were used for staining co-transfected cells: mouse anti-HA (Sigma-Aldrich, 1:500, H9658), rabbit anti-ARL13 B (Sanbio, 1:500, 17 711–1-AP) and goat-anti WASF3 (R&D systems, 1:300, AF5515). After incubation, cells were washed and incubated with the corresponding Alexa Fluor conjugated secondary antibody. Following secondary antibodies were used for single transfected cells: donkey anti-mouse, Alexa Fluor 568 (Molecular Probes, 1:500, A100037), donkey anti-rabbit, Alexa Fluor 488 (Life Technologies, 1:500, A-21206), donkey anti-goat, Alexa Fluor 568 (Molecular Probes, 1:500, A11057), goat anti-mouse, Alexa Fluor 488 (Life Technologies, 1:500, A21202) and donkey anti-rabbit, Alexa Fluor 647 (Invitrogen, 1:500, A31573). Cells on glass slides were washed three times before being mounted in Vectashield mounting medium with DAPI (Vector laboratories, VECTH-1200) on microscopy slides. Images were acquired using a Carl Zeiss Axio Imager Z2 with Apotome 2 attachment.

Statistical analysis

Statistical analyses were performed in Excel and Graph-pad/Prism 6. An ALPACA tool (version 1.53c) was used for quantification of sizes of the ciliary tip expansions (38). Error bars represent standard deviations. An unpaired t test with Welch's correction was used to compare each mutant cilium tip expansions' sizes to the wild-type. N values are stated in the figures and represent cilia. P-values are stated in the figures and symbols indicate the following P-values: ns, $P > 0.05$; $*P \leq 0.05$; $**P \leq 0.01$; $***P \leq 0.001$.

Supplementary Material

Supplementary Material is available at *HMG* online.

References

1. Young, R.W. (1967) The renewal of photoreceptor cell outer segments. *J. Cell Biol.*, **33**, 61–72.
2. May-Simera, H., Nagel-Wolfrum, K. and Wolfrum, U. (2017) Cilia – the sensory antennae in the eye. *Prog. Retin. Eye Res.*, **60**, 144–180.
3. Roepman, R. and Wolfrum, U. (2007) Protein networks and complexes in photoreceptor cilia. *Subcell. Biochem.*, **43**, 209–235.
4. Steinberg, R.H., Fisher, S.K. and Anderson, D.H. (1980) Disc morphogenesis in vertebrate photoreceptors. *J. Comp. Neurol.*, **190**, 501–518.
5. Burgoyne, T., Meschede, I.P., Burden, J.J., Bailly, M., Seabra, M.C. and Futter, C.E. (2015) Rod disc renewal occurs by evagination of the ciliary plasma membrane that makes cadherin-based contacts with the inner segment. *Proc. Natl. Acad. Sci. U. S. A.*, **112**, 15922–15927.
6. Chaitin, M.H. and Burnside, B. (1989) Actin filament polarity at the site of rod outer segment disk morphogenesis. *Invest. Ophthalmol. Vis. Sci.*, **30**, 2461–2469.
7. Nishimura, D.Y., Baye, L.M., Perveen, R., Searby, C.C., Avila-Fernandez, A., Pereiro, I., Ayuso, C., Valverde, D., Bishop, P.N., Manson, F.D. *et al.* (2010) Discovery and functional analysis of a retinitis pigmentosa gene, C2ORF71. *Am. J. Hum. Genet.*, **86**, 686–695.
8. Collin, R.W., Safieh, C., Littink, K.W., Shalev, S.A., Garzozi, H.J., Rizel, L., Abbasi, A.H., Cremers, F.P., den Hollander, A.I., Klevering, B.J. *et al.* (2010) Mutations in C2ORF71 cause autosomal-recessive retinitis pigmentosa. *Am. J. Hum. Genet.*, **86**, 783–788.
9. Corral-Serrano, J.C., Lamers, I.J.C., van Reeuwijk, J., Duijkers, L., Hoogendoorn, A.D.M., Yildirim, A., Argyrou, N., Ruigrok, R.A.A., Letteboer, S.J.F., Butcher, R. *et al.* (2020) PCARE and WASF3 regulate ciliary F-actin assembly that is required for the initiation of photoreceptor outer segment disk formation. *Proc. Natl. Acad. Sci. U. S. A.*, **117**, 9922–9931.
10. Suetsugu, S., Miki, H. and Takenawa, T. (1999) Identification of two human WAVE/SCAR homologues as general actin regulatory molecules which associate with the Arp2/3 complex. *Biochem. Biophys. Res. Commun.*, **260**, 296–302.
11. Spencer, W.J., Lewis, T.R., Phan, S., Cady, M.A., Serebrovskaya, E.O., Schneider, N.F., Kim, K.-Y., Cameron, L.A., Skiba, N.P., Ellisman, M.H. *et al.* (2019) Photoreceptor disc membranes are formed through an Arp2/3-dependent lamellipodium-like mechanism. *Proc. Natl. Acad. Sci. U. S. A.*, **116**, 27043–27052.
12. Oldfield, C.J., Xue, B., Van, Y.Y., Ulrich, E.L., Markley, J.L., Dunker, A.K. and Uversky, V.N. (2013) Utilization of protein intrinsic disorder knowledge in structural proteomics. *Biochim. Biophys. Acta*, **1834**, 487–498.
13. Kumar, M., Michael, S., Alvarado-Valverde, J., Mészáros, B., Sámano-Sánchez, H., Zeke, A., Dobson, L., Lazar, T., Örd, M., Nagpal, A. *et al.* (2022) The eukaryotic linear motif resource: 2022 release. *Nucleic Acids Res.*, **50**, D497–D508.

14. Ward, J.J., McGuffin, L.J., Bryson, K., Buxton, B.F. and Jones, D.T. (2004) The DISOPRED server for the prediction of protein disorder. *Bioinformatics*, **20**, 2138–2139.

15. Jumper, J., Evans, R., Pritzel, A., Green, T., Figurnov, M., Ronneberger, O., Tunyasuvunakool, K., Bates, R., Žídek, A., Potapenko, A. *et al.* (2021) Highly accurate protein structure prediction with AlphaFold. *Nature*, **596**, 583–589.

16. McGuffin, L.J., Bryson, K. and Jones, D.T. (2000) The PSIPRED protein structure prediction server. *Bioinformatics*, **16**, 404–405.

17. Guan, X. and Fierke, C.A. (2011) Understanding protein Palmitoylation: biological significance and enzymology. *Sci. China Chem.*, **54**, 1888–1897.

18. Pauling, L., Corey, R.B. and Branson, H.R. (1951) The structure of proteins: two hydrogen-bonded helical configurations of the polypeptide chain. *Proc. Natl. Acad. Sci. U. S. A.*, **37**, 205–211.

19. Emmer, B.T., Souther, C., Toriello, K.M., Olson, C.L., Epting, C.L. and Engman, D.M. (2009) Identification of a palmitoyl acyltransferase required for protein sorting to the flagellar membrane. *J. Cell Sci.*, **122**, 867–874.

20. Kumeta, M., Panina, Y., Yamazaki, H., Takeyasu, K. and Yoshimura, S.H. (2018) N-terminal dual lipidation-coupled molecular targeting into the primary cilium. *Genes Cells*, **23**, 715–723.

21. Omori, Y., Chaya, T., Katoh, K., Kajimura, N., Sato, S., Muraoka, K., Ueno, S., Koyasu, T., Kondo, M. and Furukawa, T. (2010) Negative regulation of ciliary length by ciliary male germ cell-associated kinase (Mak) is required for retinal photoreceptor survival. *Proc. Natl. Acad. Sci. U. S. A.*, **107**, 22671–22676.

22. Haffner, C., Jarchau, T., Reinhard, M., Hoppe, J., Lohmann, S.M. and Walter, U. (1995) Molecular cloning, structural analysis and functional expression of the proline-rich focal adhesion and microfilament-associated protein VASP. *EMBO J.*, **14**, 19–27.

23. Ball, L.J., Jarchau, T., Oschkinat, H. and Walter, U. (2002) EVH1 domains: structure, function and interactions. *FEBS Lett.*, **513**, 45–52.

24. Gertler, F.B., Niebuhr, K., Reinhard, M., Wehland, J. and Soriano, P. (1996) Mena, a relative of VASP and drosophila enabled, is implicated in the control of microfilament dynamics. *Cell*, **87**, 227–239.

25. Chapple, J.P., Hardcastle, A.J., Grayson, C., Willison, K.R. and Cheetham, M.E. (2002) Delineation of the plasma membrane targeting domain of the X-linked retinitis pigmentosa protein RP2. *Invest. Ophthalmol. Vis. Sci.*, **43**, 2015–2020.

26. Navarro-Lérida, I., Alvarez-Barrientos, A., Gavilanes, F. and Rodriguez-Crespo, I. (2002) Distance-dependent cellular palmitoylation of de-novo-designed sequences and their translocation to plasma membrane subdomains. *J. Cell Sci.*, **115**, 3119–3130.

27. Resh, M.D. (2013) Covalent lipid modifications of proteins. *Curr. Biol.*, **23**, R431–R435.

28. Dominguez, R. (2009) Actin filament nucleation and elongation factors–structure-function relationships. *Crit. Rev. Biochem. Mol. Biol.*, **44**, 351–366.

29. Hwang, T., Parker, S.S., Hill, S.M., Ilunga, M.W., Grant, R.A., Mouneimne, G. and Keating, A.E. (2021) A distributed residue network permits conformational binding specificity in a conserved family of actin remodelers. *elife*, **10**, e70601.

30. Afanasyeva, T.A.V., Corral-Serrano, J.C., Garanto, A., Roepman, R., Cheetham, M.E. and Collin, R.W.J. (2021) A look into retinal organoids: methods, analytical techniques, and applications. *Cell. Mol. Life Sci.*, **78**, 6505–6532.

31. Procter, J.B., Carstairs, G.M., Soares, B., Mourão, K., Ofoegbu, T.C., Barton, D., Lui, L., Menard, A., Sherstnev, N., Roldan-Martinez, D. *et al.* (2021) Alignment of biological sequences with Jalview. *Methods Mol. Biol.*, **2231**, 203–224.

32. Prehoda, K.E., Lee, D.J. and Lim, W.A. (1999) Structure of the enabled/VASP homology 1 domain-peptide complex: a key component in the spatial control of actin assembly. *Cell*, **97**, 471–480.

33. Howard, C.J., Hanson-Smith, V., Kennedy, K.J., Miller, C.J., Lou, H.J., Johnson, A.D., Turk, B.E. and Holt, L.J. (2014) Ancestral resurrection reveals evolutionary mechanisms of kinase plasticity. *elife*, **3**, e04126.

34. Mészáros, B., Erdos, G. and Dosztányi, Z. (2018) IUPred2A: context-dependent prediction of protein disorder as a function of redox state and protein binding. *Nucleic Acids Res.*, **46**, W329–w337.

35. Varadi, M., Anyango, S., Deshpande, M., Nair, S., Natassia, C., Yordanova, G., Yuan, D., Stroe, O., Wood, G., Laydon, A. *et al.* (2022) AlphaFold protein structure database: massively expanding the structural coverage of protein-sequence space with high-accuracy models. *Nucleic Acids Res.*, **50**, D439–D444.

36. Torres, J.Z., Miller, J.J. and Jackson, P.K. (2009) High-throughput generation of tagged stable cell lines for proteomic analysis. *Proteomics*, **9**, 2888–2891.

37. Schindelin, J., Arganda-Carreras, I., Frise, E., Kaynig, V., Longair, M., Pietzsch, T., Preibisch, S., Rueden, C., Saalfeld, S., Schmid, B. *et al.* (2012) Fiji: an open-source platform for biological-image analysis. *Nat. Methods*, **9**, 676–682.

38. Doornbos, C., van Beek, R., Bongers, E., Lugtenberg, D., Klaren, P.H.M., Vissers, L., Roepman, R. and Oud, M.M. (2021) Cell-based assay for ciliopathy patients to improve accurate diagnosis using ALPACA. *Eur. J. Hum. Genet.*, **29**, 1677–1689.